



Contents lists available at ScienceDirect

Arabian Journal of Chemistry

journal homepage: www.ksu.edu.sa

Original article

Preparation of S-doped biochar with sodium thiosulfate as activator and sulfur source and its highly efficient adsorption for Hg^{2+} Zengrun Xie^a, Yuanyuan Zhang^b, Shengxiao Zhang^{a,*}, Hou Chen^a, Chenyu Du^a, Caijuan Zhong^a^a School of Chemistry and Materials Science, Institute of Environmental Science, Ludong University, Yantai 264025, Shandong Province, China^b Environmental Monitor Station of Yantai, No. 118, Qingnian South Road, Yantai 264000, Shandong Province, China

ARTICLE INFO

Keywords:

Cherry stone
Sulfur-doped biochar
Mercury Adsorption
Coordination interaction
Membrane filtration device

ABSTRACT

Sulfur-doped biochar (S_4BC) was prepared with cherry kernel powder as carbon source, $\text{Na}_2\text{S}_2\text{O}_3$ as sulfur source and chemical activator. $\text{Na}_2\text{S}_2\text{O}_3$ can activate biochar through the reaction with carbon, intercalation of alkali metals and the generated gas rushing out of pores, and at the same time, active sulfur atoms are doped into biochar during pyrolysis. The physical and chemical properties of S_4BC adsorbent were evaluated by various characterization techniques. The results show that S_4BC calcined at $800\text{ }^\circ\text{C}$ has huge specific surface area of $959.6\text{ m}^2/\text{g}$, developed pore structure, and high content of S (18.84 wt%). Moreover, due to the existence of sulfur and oxygen functional groups, $\text{S}_4\text{BC-800}$ provides sufficient active sites for the adsorption of Hg^{2+} . According to Langmuir model, the maximum adsorption capacity of $\text{S}_4\text{BC-800}$ for Hg^{2+} is 724 mg/g at 313 K , and the adsorption speed is fast with excellent stability and reusability. The microfiltration membrane device based on $\text{S}_4\text{BC-800}$ can effectively remove the low concentration of Hg^{2+} in the solution. In this study, a simple method for preparing SBC materials is developed, which is not only of great significance as an adsorbent for Hg^{2+} , but also provides a new choice for the preparation of heteroatom-doped materials.

1. Introduction

Heavy metals are common pollutants in soil and water environment. Unlike organic pollutants, heavy metals are non-biodegradable and often accumulate in organisms. Many heavy metal ions are known to be high toxic, among which mercury is considered to be one of the most common and dangerous heavy metals in water. In the list of dangerous compounds, mercury ranks the sixth among the most toxic chemicals, and it has been proved to be readily bioaccumulative (Kou et al., 2021). According to the regulations of the US Environmental Protection Agency, mercury is listed as one of the priority pollutants (Liu et al., 2018a). Once mercury enters the food chain, this element will accumulate in humans and animals, causing many adverse effects on their health, for example, emotional and mental degradation, blindness, and loss of consciousness (Wang et al., 2022), the mercury concentration in Arctic marine animals is about 12–1800 times higher than that before industrialization (about 10 years ago) (Yang et al., 2020) and the notorious Minamata Bay incident in Japan from 1953 to 1956 is also a typical ecological accident of mercury pollution (Liu et al., 2018a). Divalent

mercury ion (Hg^{2+}) is the main existing form of mercury in water, and even ultra-trace Hg^{2+} will destroy the central nervous system and may lead to death (Clarkson and Magos, 2006). Therefore, in order to avoid the harm to human health and prevent the continuous pollution of limited fresh water resources by Hg^{2+} , it is very important to develop advanced Hg^{2+} removal technology for reducing health risks and ensuring ecological security.

Nowadays, many technologies have been used to remove Hg^{2+} from polluted water, such as precipitation (Wang et al., 2019a), ion exchange (Saleem et al., 2019), biofilm treatment (Castro-Munoz et al., 2021), electrochemistry (Wu et al., 2019), and adsorption (Fu et al., 2022). Among them, adsorption is considered as one of the most reliable technologies to remove Hg^{2+} from water because of the advantages of simple operation, high removal efficiency, strong adaptability, and low cost, and it can effectively treat Hg^{2+} in sewage and meet the discharge standards. In addition, adsorption is sometimes reversible, so the adsorbent can be regenerated through proper desorption process, which greatly saves the resource and reduces the cost. Therefore, adsorption is recognized as an effective and economical method to treat wastewater

* Corresponding author at: Ludong University, School of Chemistry and Materials Science, Yantai 264025, China.

E-mail address: beijingzxsx@163.com (S. Zhang).<https://doi.org/10.1016/j.arabjc.2024.105955>

Received 23 April 2024; Accepted 6 August 2024

Available online 11 August 2024

1878-5352/© 2024 Published by Elsevier B.V. on behalf of King Saud University. This is an open access article under the CC BY-NC-ND license (<http://creativecommons.org/licenses/by-nc-nd/4.0/>).

containing Hg^{2+} , which is widely used in the field of environmental sewage treatment (Vikrant and Kim, 2019). The adsorbents used to treat Hg^{2+} in wastewater include carbon material, polymeric adsorbents, and biological material, among which carbon-based materials, for example, activated carbon, biomass-derived carbon, graphene oxide and carbon nanotubes, have been widely adopted because of their excellent performance for Hg^{2+} adsorption in water (Hussain et al., 2020).

Biochar prepared by pyrolysis of various biomass is considered as one of the priority adsorbents to eliminate Hg^{2+} pollution because of its developed internal pore structure, huge surface area and rich functional groups (Giri et al., 2021). Usually, biochar materials obtained by direct pyrolysis have the disadvantages of poor porosity and small specific surface area (Abbas et al., 2018). Physical or chemical methods can be used to make holes and promote the specific surface area. Physical activation method refers to the method of preparing porous carbon materials by activating materials with gases such as water vapor and CO_2 at high temperature (900 °C). However, the obtained porous carbon is not very large in specific surface area and pore volume, and the energy consumption in the preparation process is relatively high (Godlewska et al., 2019). Compared with physical activation, chemical activating reagents can erode the surface of carbon, leaving nano-scale cracks, that is, micropores or mesopores structure, which endows the advantages of developed pore structure, high specific surface area, low energy consumption, and easily controllable reaction. In the reported research, HNO_3 (Wepasnick et al., 2011), KOH (Srinivasan et al., 2019), CuCl_2 (Liu et al., 2018b), and KHCO_3 (Qu et al., 2020) are all used as chemical activators. In the process of activation of biochar materials, the activator reacts with tar and amorphous carbon in biomass framework to achieve opening holes. Subsequently, the activator continues to corrode the carbon on the inner surface of the pores, and the generated CO_2 and CO are discharged. The original pores are further enlarged from the original micropores to mesopores or macropores, thus creating interconnected pore structure and high specific surface area. Taking KOH as an example, in the activation process, in addition to the gas generated by the reaction between KOH and carbon escaping at high temperature to form pores, metal potassium also expands the lattice of carbon through intercalation, and pores can be formed in the structure of carbon after washing with acid solution to remove potassium, thus achieving the purpose of pore formation. However, due to the limitations of the reported study, such as multiple synthetic steps, harsh treatment conditions, small specific surface area, limited active sites, low adsorption capacity, slow adsorption rate and relatively poor reuse performance (He et al., 2016), the adsorption performance of biochar material for Hg^{2+} needs to be further improved.

To extend functionality of carbon material, it has been proved that doping heteroatom (such as N, F, S, B and P) into biochar can improve their adsorption and catalysis properties. Compared with other heteroatoms, sulfur atoms have many attractive characteristics, such as large atomic radius (Liang et al., 2019), low electronegativity (Ma et al., 2022), soft base feature, and various functional groups. These characteristics make it play a unique role in the adsorption of Hg^{2+} in solution. At present, the heteroatom doping in biochar material is mainly to calcine the mixture of carbon precursor and heteroatom dopant at high temperature under inert atmosphere, which can be subdivided into one-step method (co-pyrolysis of precursor and chemical activator) and two-step method (carbonization of biomass and activation of activator). In contrast, the two-step method is easier to realize, because the first pyrolysis stage is usually carried out at a lower temperature, so it can obtain high yield of biomass charcoal. Subsequently, biochar with relatively poor porosity can be further gasified with activator to form a large number of new pores (Hu et al., 2021).

Many cherry stones will be left in the consumption of cherries, as well as in the production of preserved fruits, fruit wine and canned food, which has potential threat to the environment and urgently needs appropriate methods for comprehensive utilization. Previous reports show that cherry core belongs to lignocellulosic waste with dense

structure, which is mainly composed of cellulose, lignin and hemicellulose (Yilmaz et al., 2019). Lignin-rich biomass can be carbonized or activated in inert atmosphere to produce highly porous biochar with large surface area (Correa et al., 2017; Wang et al., 2017). Sodium thiosulfate pentahydrate ($\text{Na}_2\text{S}_2\text{O}_3 \cdot 5\text{H}_2\text{O}$) owns some properties of chemical activator, for example, reactivity with carbon, intercalation of alkali metal, decomposability of heating, and it also contains an active sulfur atom, which is liable to be inserted into lattice of various material. Therefore, if $\text{Na}_2\text{S}_2\text{O}_3$ is used as activator for preparation biochar, it can not only achieve the purpose of pore formation by activation but also attain S atoms doping simultaneously to get S-doped biochar (SBC) material. According to Pearson's hard soft acid-base theory (HSAB) (Pearson, 1963), SBC containing S functional groups, as a kind of soft base, can be expected to own high affinity for Hg^{2+} (soft acid). Therefore, based on the above analysis, we try to use cherry kernel powder as carbon source and $\text{Na}_2\text{S}_2\text{O}_3 \cdot 5\text{H}_2\text{O}$ as sulfur source and activator to prepare SBC for Hg^{2+} adsorption. The effects of key synthesis conditions, for example, pyrolysis temperature, mass ratio of $\text{Na}_2\text{S}_2\text{O}_3 \cdot 5\text{H}_2\text{O}$ to biochar, on properties of SBC were studied in detail. The surface morphology and chemical properties of SBC were comprehensively characterized. Through the systematic study of pH dependence, kinetics, isotherm, thermodynamic properties, desorption and regeneration ability, the adsorption performance of Hg^{2+} was evaluated. The possible mechanism of mercury adsorption by SBC was also discussed. To our knowledge, this is the first time that $\text{Na}_2\text{S}_2\text{O}_3$ is used as activator and sulfur source to prepare SBC material for Hg^{2+} removal, which simplifies the process to select appropriate chemical compounds and corresponding ratio as activator and heteroatom source.

2. Materials and methods

2.1. Chemicals and reagents

The reagents used in the experiment are analytical pure reagents, which have not been further purified. The mercury reserve solution with a concentration of 1 g/L was prepared by dissolving HgCl_2 (purchased from Jiangyan Huanqiu Chemical Reagent Company, Jiangsu Province) in pure water. $\text{Na}_2\text{S}_2\text{O}_3 \cdot 5\text{H}_2\text{O}$, HCl and NaOH are provided by Tianjin Comel Chemical Reagent Co. Ultrapure water used in experiment was prepared by ULUPURE water purification system (Chengdu, Sichuan, China).

2.2. Synthetic approach of the SBC

The cherry kernel powder of 80 mesh placed in a corundum crucible was heated to 500 °C in a tubular furnace under nitrogen atmosphere at a heating rate of 10 °C/min, and then maintained for 2 h. The biochar (BC) was obtained and used in next experiments.

For activation and sulfur doping, 1.0 g BC was mixed with a certain amount of $\text{Na}_2\text{S}_2\text{O}_3 \cdot 5\text{H}_2\text{O}$ (0.5 g, 1.0 g, 2.0 g, 4.0 g, 5.0 g) and fully ground, and then transferred to a corundum crucible. The mixture was heated to 500 °C, 600 °C, 700 °C, 800 °C and 900 °C at a heating rate of 5 °C/min in nitrogen atmosphere, and then kept for two hours. The obtained material was washed with 1 mol/L HCl and deionized water until the pH value was 7, and then most of the water was removed by vacuum filtration. Finally, the materials were dried at 90 °C for 24 h, and marked as sulfur-doped biochar ($\text{S}_x\text{BC}-Y$, where X represents the weight ratio of BC to $\text{Na}_2\text{S}_2\text{O}_3 \cdot 5\text{H}_2\text{O}$ and Y represents the activation temperature). The ingredients list of $\text{S}_x\text{BC}-Y$ is shown in Table 1. The yield was calculated by the ratio of final weight of product to the origin mass of BC.

2.3. Characterization of adsorbents

The specific surface area and pore size were analyzed by ASAP2460 instrument (Micromeritics Instruments Corporation, USA), and the

Table 1

Elemental analysis, BET specific surface areas, average pore size, and product yield of various materials.

Absorbent	Elemental composition (wt%)			SBET (m ² /g)	Average pore size (nm)	Product yield (%)
	C	H	S			
BC	76.04	2.70	0.03	1.76	/	/
S ₄ BC-500	53.87	1.44	19.99	82.81	2.05	92.61
S ₄ BC-600	51.66	1.54	21.76	358.14	2.08	78.73
S ₄ BC-700	57.44	1.24	20.88	644.26	2.26	38.81
S ₄ BC-800	65.56	0.73	18.84	959.63	2.57	30.25
S ₄ BC-900	72.24	0.74	11.05	1303.07	2.31	24.41

samples were degassed in vacuum at 120 °C for 6 h before analysis. The specific surface area is calculated by Brunauer Emmett Teller (BET) equation and the pore size distribution is calculated by Barret Joyner Halenda (BJH) model. X-ray photoelectron spectroscopy (XPS) analysis adopts Thermo ESCALAB 250XI instrument (Thermo Fisher Scientific, USA), using monochromatic Al K α source, and the binding energy is calibrated at C1s 284.8 eV. Scanning electron microscope (SEM, Hitachi, Japan) was used to observe the surface morphology of BC and S₄BC-800. X-ray diffraction (XRD) analysis is carried out on an Rigaku D/max-2500 instrument (Nippon Corporation, Japan), and the radiation source is Cu K α ray, and the scanning range is 10–80° with the scanning speed of 10°/min. Fourier transform infrared spectroscopy (FT-IR) analysis adopts American PerkinElmer Spectrum FT-IR instrument, using potassium bromide tableting method, and deducts potassium bromide background and air background. Raman spectrometer (Renishaw Invia, UK) was used to measure the Raman spectra of materials excited by 532 nm laser. Elemental analysis (C, H, S) was performed on an Elementar Vario EL III analyzer (Elementar Analysensysteme Comp., Hanau, Germany).

2.4. Batch adsorption experiments

2.4.1. Adsorption studies

The Hg²⁺ adsorption experiments were carried out in a 100 mL polypropylene bottle with solution volume of 50 mL. After the solution pH is adjusted to the set value with NaOH or HCl solution, the suspension is placed in a thermostatic oscillator at 30 °C for 6 h to study the effect of solution pH on mercury adsorption. The adsorption isotherm of mercury was measured by changing the initial concentration of mercury (20–300 mg/L).

2.4.2. Study on adsorption kinetics and adsorption isotherm

To study the adsorption kinetics, experiments were carried out in a 100 mL polypropylene bottle with a solution volume of 50 mL. The pH value was 6.5, and the initial concentration of Hg²⁺ was set at 100, 180 and 300 mg/L. The sampling time interval is 10, 20, 30, 60, 90, 120, 180, 240, and 300 min. In order to study the adsorption behavior of Hg²⁺ on adsorbents, quasi-first-order kinetic model and quasi-second-order kinetic model were used to fit the data. These models can provide important information about the distribution of adsorbate molecules on the solid/liquid interface, and their linear equations are as follows.

$$\log(q_e - q_t) = \log q_e - \frac{k_1 t}{2.303} \quad (1)$$

$$\frac{t}{q_t} = \frac{1}{k_1 q_e^2} + \frac{t}{q_e} \quad (2)$$

where q_t is the adsorption capacity (mg/g) of pollutant Hg²⁺ at any time, and q_e is the equilibrium adsorption capacity (mg/g); α is the initial adsorption rate; k_1 and k_2 are the adsorption rate constants of pseudo-first-order and pseudo-second-order adsorption kinetic models, respectively. The value of q_e (mg/g), α (mg/g min), k_1 (min⁻¹), and k_2 (g/mg min) can be calculated from the slope and intercept of the linear fitting

of Eqs. (1) and (2). When t tends to 0, the original adsorption rate can be defined as q_t/t . The initial adsorption rate h (mg/g min) can be described by the following equation:

$$h = k q_e^2 (t \rightarrow 0) \quad (3)$$

The adsorption isotherm of mercury was measured by changing the initial concentration of mercury (20–300 mg/L). In this study, Langmuir and Freundlich adsorption isotherm models were used to fit the equilibrium adsorption data. Langmuir isothermal adsorption model is usually used for monolayer adsorption, in which a large number of adsorption sites have the same affinity with adsorbates, while Freundlich isothermal adsorption model is mainly used to describe the heterogeneous adsorption process (Zheng et al., 2018), and their linear equations are as follows (Eqs. (4) and (5)).

$$\frac{c_e}{q_e} = \left(\frac{1}{q_{\max} b} \right) + \frac{c_e}{q_{\max}} \frac{c_e}{q_e} = \frac{1}{q_{\max} b} + \frac{c_e}{q_{\max}} \quad (4)$$

$$\log q_e = \log K_F + \frac{1}{n} \log c_e \quad (5)$$

where q_e (mg/g) and q_{\max} (mg/g) represent the equilibrium adsorption capacity and maximum adsorption capacity of adsorbent S₄BC-800, and q_{\max} (mg/g) can be calculated from the slope of the line fitting by c_e/q_e to c_e ; c_e (mg/L) represents the equilibrium concentration of adsorbent; b (L/mg) is the equilibrium adsorption constant. Here, K_F (mL^{1/n} μg^{1-1/n}) and n are Freundlich constants, indicating adsorption capacity.

2.4.3. Interference experiment and reuse

To study the adsorption kinetics, the sampling time interval is 10, 20, 30, 60, 90, 120, 180, 240, and 300 min. K⁺, Na⁺ and Ca²⁺ were added into the solution to study the effect of coexisting ions on the adsorption of mercury. After the adsorption, the solution was taken and centrifuged for ten minutes at 10000 rpm. The concentration of Hg²⁺ in the supernatant was measured by atomic absorption spectrometer (AA240, Varian, USA). If the concentration of Hg²⁺ is lower than 1 mg/L, a mercury vapor analyzer (Leeman labs, Hydra II, USA) is used to determine its concentration.

Hydrochloric acid solution (0.2 mol/L) containing thiourea (3 %) is used to desorb Hg²⁺. After the Hg²⁺ adsorption is completed, the adsorbent is separated by centrifuge and mixed with the eluent, and then put into a thermostatic oscillator to shake for 2 h. The adsorbent was separated and washed with pure water several times, and then used in the next adsorption experiment to investigate their reusability.

3. Results and discussion

3.1. Characterization of S_xBC-Y

The ratio of activator to raw BC may affect the morphology and pore structure of SBC materials, and SEM images of S_xBC-800 with different proportion of Na₂S₂O₃·5H₂O are shown in Fig. S1 (a–d). It can be seen that the morphology of BC is relatively smooth, and seldom pores appear on the surface. With the weight ratio of Na₂S₂O₃·5H₂O increasing, the roughness and pores of the materials enhance obvious, indicating that as a chemical activator, more Na₂S₂O₃·5H₂O will create more pores by reaction with BC. Especially, when the weight ratio of Na₂S₂O₃·5H₂O to BC is 4:1 (Fig. S1c), well-developed macropores are generated with randomly distributed micropores in stacked and folded irregular layers. Fig. S1(d) shows that excessive Na₂S₂O₃·5H₂O (5:1) will result in the collapse of carbon skeleton structure and destroy of micropores, which may lead to the decrease of its adsorption performance. Thus, the weight ratio 4:1 of Na₂S₂O₃·5H₂O to BC is selected for next experiments.

Pyrolysis temperature is another key factor to affect the property of the SBC materials. Fig. 1(a–f) shows SEM images of BC and S₄BC-Y under different reaction temperature. Compared with BC, S₄BC-500 and S₄BC-

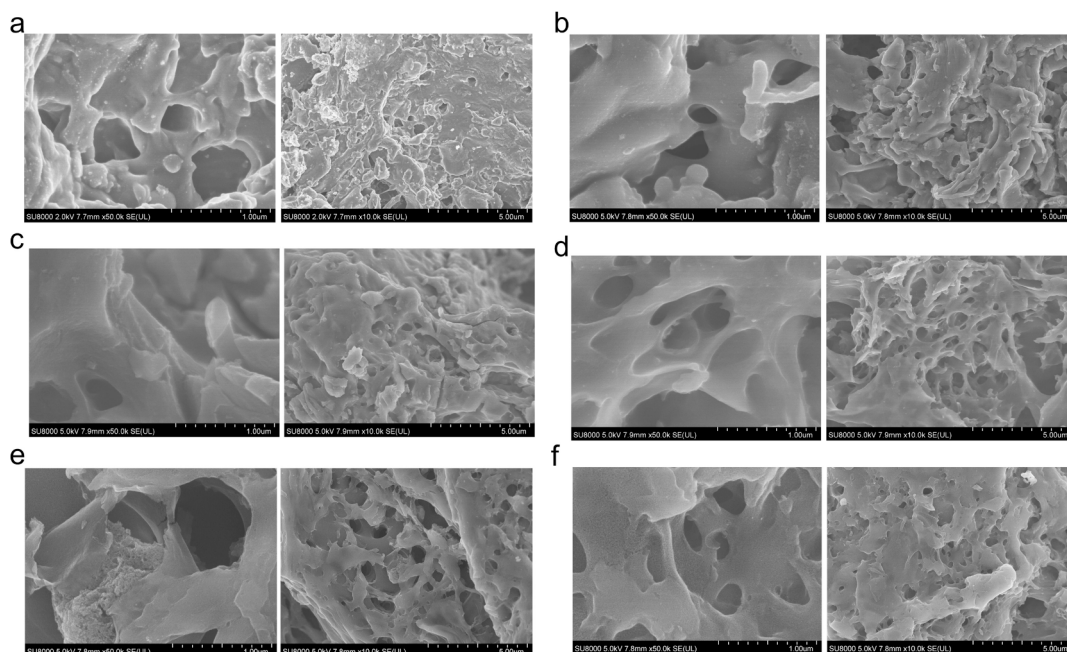


Fig. 1. SEM images of (a) BC, (b) S₄BC-500, (c) S₄BC-600, (d) S₄BC-700, (e) S₄BC-800 and (f) S₄BC-900

600 exhibit some pores on the surface, but the pores are shallow and not interconnected each other, indicating the weak activation ability under low temperature. When the reaction temperature is elevated over 700 °C, a great deal of developed and inter-connected macropores with stacking and folding can be observed on S₄BC-700, S₄BC-800, and S₄BC-900, and even plenty of micropores and mesoporous pores occur on the side wall of macropores (Fig. S2), which will lead to high specific surface area and provide abundant active sites for adsorption. This is mainly because the pyrolysis and reaction with BC of Na₂S₂O₃ at high temperature produce hierarchical pore structure.

The specific surface area and pore size are further investigated, and the N₂ adsorption–desorption diagrams and pore size distributions are shown in Fig. 2 and Fig. S3. The N₂ adsorption–desorption diagram of BC conforms to type II of non-porous or macroporous adsorption structure (Qu et al., 2021), while that of S₄BC-800 belongs to type I, and at low relative pressure (P/P_0), it has a clear platform and a large N₂ adsorption capacity, and then a narrow hysteresis loop appears in the range of P/P_0 of 0.4–1.0, indicating that there are abundant micropores and a small number of mesopores and macropores (Li et al., 2016), which is consistent with the SEM results. Generally, activated carbon with definite pore size distribution can be produced by activation with chemical

activator. For further proof, the pore size distribution of S₄BC is shown in inset of Fig. 2(b). It can be seen that all sulfur-doped activated carbons are bimodal, and the pore sizes mainly composed of micropores (<0.8 nm) and certain mesopores (2–3 nm), which is consistent with the adsorption isotherm of N₂. Table 1 shows the detailed information of specific surface area, element content, product yield and porosity. Macropores are very important if biochar is used as an adsorbent to remove pollutants in water or as an electrode in energy storage system. They act as carriers for the solution to pass through pores until it reaches micropores and mesopores (dos Reis et al., 2021, 2024). The prepared S₄BC has a certain amount of macropores and abundant micropores, which can further improve the adsorption of mercury ions. The yield of S₄BC decreased with the increase of preparation temperature, and it decreased from 92.61 % at 500 °C to 24.41 % at 900 °C. This is mainly because the reaction between carbon in BC and Na₂S₂O₃ will produce carbon sulfide and carbon oxide at high temperature, and the water and organic matter in BC will volatilize, resulting in carbon weight loss. The surface area of BC is very low (only 1.76 m²/g), indicating the lack of pore structure. When the BC is activated by Na₂S₂O₃ under different temperature, the surface area enhanced significantly, indicating the pivotal role of Na₂S₂O₃ for pore formation. With the reaction

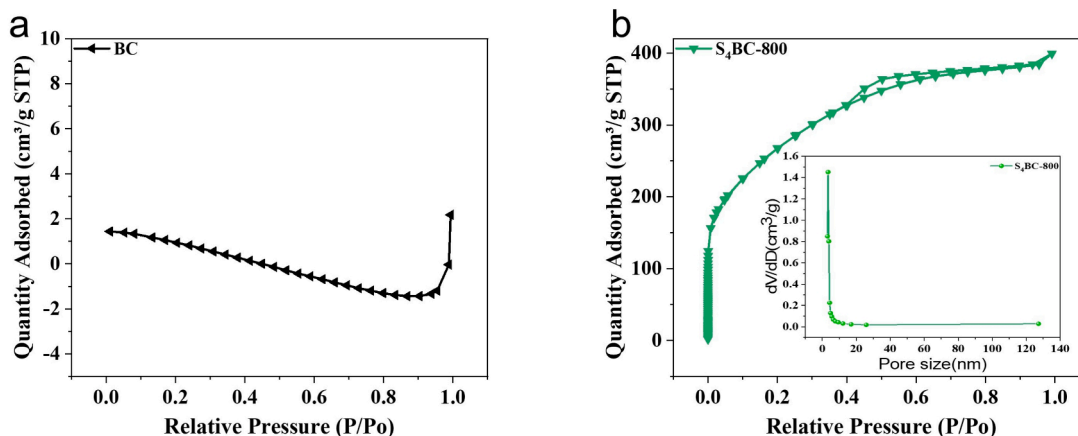


Fig. 2. N₂ adsorption–desorption isotherms of (a) BC and (b) S₄BC-800, and (inset of b) pore size distributions of S₄BC-800

temperature increasing from 500 to 900 °C, the surface area of S₄BC boosts rapidly from 82.8 to 1303.1 m²/g, which may result from the strong reactivity between BC and Na₂S₂O₃ under high temperature, and the promotion of surface area will be conducive to improve the adsorption property of material. As for elemental composition, with the activation temperature increasing from 500 °C to 800 °C, the sulfur content is relatively steady (about 20 wt%), while it decreases sharply to 11.05 % when temperature up to 900 °C, which results from the pyrolysis of S-containing groups under too high temperature (Guo et al., 2018). Compared with previous studies on S-doped carbon (Guo et al., 2017; Park et al., 2014; Seredych and Bandoz, 2011; Yang et al., 2021; Zeng et al., 2018), S₄BC shows a high amount S-doping, which will contribute to create more adsorption sites. The results demonstrate dual functions of Na₂S₂O₃ on activation pore-forming and S-doping during S₄BC material preparation.

According to the above description, it can be inferred that there are two main mechanisms for the activation of Na₂S₂O₃·5H₂O: Firstly, Na₂S₂O₃·5H₂O loses its crystal water and becomes anhydrous sodium thiosulfate; Then, Na₂S₂O₃ will consume a certain amount of BC to generate hydrogen sulfide, sulfur dioxide, water, sodium sulfate, and oxygen. Part of the gas rushes out of BC, causing BC to break or form larger holes for preliminary pore-making, and in this process, S atoms are bonded to the carbon skeleton through covalent bonds, which is partly carried out under the catalysis of alkali metal Na. In the second part, Na⁺ is reduced to free metal Na, and it enters the carbon grid. Through the insertion of metal Na, the carbon grid expands, and the inserted substances in the carbon matrix are quickly removed, thus forming a large number of pores. After the residue is removed by acid washing, numerous micropores are formed in the carbon framework to complete the process of activation and pore-making.

The XRD patterns of BC and S₄BC are shown in Fig. 3(a). It can be seen that all samples have two broad diffraction peaks near 24° and 44°, which correspond to the characteristics of (002) and (100) planes of graphite (Ma et al., 2013), indicating that graphitization occurred in the process of carbonization and activation of these materials. The relatively low graphitization degree of S₄BC indicates that the addition of sulfur may destroy the graphitization structure of BC to some extent, thus increasing the number of defects, which may generate more active sites and promote the adsorption performance. Compared with BC and S₄BC-500 samples, the diffraction peaks of impurities in S₄BC materials prepared at other temperatures are not obvious, indicating that high activation temperature is helpful to remove impurities. The sum Raman spectra of BC and S₄BC also show that sulfur doping can deform the carbon skeleton and produce more defects, which can enhance the adsorption performance of S₄BC for mercury ions (Text S1 and Fig. S4).

The FT-IR spectra of BC and S₄BC also confirmed the successful doping of sulfur. As can be seen from Fig. 3(b), the FT-IR spectra of all materials show a peak at 3800 cm⁻¹, which is attributed to the joint action of O—H bond and O—H stretching vibration (Li et al., 2018a). In comparison, the tensile vibration from O=S=O (1155 cm⁻¹) is

observed only at SBC, which was caused by sulfur oxide (Guo et al., 2018), and the peak is apparent when the pyrolysis temperature is below 800 °C, while it shrinks sharply under temperature of 900 °C, indicating the decomposition of the S-containing groups at high temperature, which is in accord with the decrease of sulfur content from elemental analysis (Table 1). The S₄BC-500 shows the C-S tensile vibration peak located at 785 cm⁻¹ from thiophene sulfur (Uygun et al., 2009), while the peak disappears when the pyrolysis temperature is over 600 °C due to the destroy of the groups. C—O and C—C stretching vibration on saturated carbon at 2668 cm⁻¹, O—C—O stretching vibration at 1577 cm⁻¹ and C=O stretching vibration peaks at 2102 cm⁻¹ are also observed, which indicate that the prepared SBC adsorbent contained abundant oxygen-containing functional groups on the surface of the material. Sulfur and oxygen functional groups will be conducive to coordinate with Hg²⁺.

Generally speaking, the adsorption properties of carbonaceous materials are closely related to their chemical composition and surface properties, especially the functional groups containing nitrogen and sulfur (Wang et al., 2015; Yang et al., 2012), so the elemental composition and chemical valence states of S₄BC and BC were characterized by XPS. As shown in Fig. 4(a), the XPS survey spectrum of BC exhibits C and O elements, and no S peak is detected, indicating that the raw material of cherry stone contains no S element. While all S₄BC materials show peaks of C, O and S element. The C peak appears because BC and S₄BC are mainly composed of C, and the S peak in S₄BC demonstrates that S element has been successfully doped into carbon skeleton. In order to highlight the surface C, O, and S configurations in the sample, the high-resolution XPS spectra of C 1s, O 1s and S 2p (S₄BC-800) are deconvoluted and divided into several peaks. As shown in Fig. 4(b), the high-resolution spectrum of C 1s has four peaks at 284.6, 285.6, 287.3, and 290.02 eV, which result from graphite and aliphatic carbon (C—C/C=C, 72.16 %), alcohol or ether group (C—O, 14.93 %), carbonyl group (—C=O—, 6.13 %), and carboxyl or ester group (O—C=O, 6.78 %), respectively (Li et al., 2018b). In Fig. 4(c) of O 1s, peaks were observed at 530.68 eV, 531.78 eV, and 532.68 eV, corresponding to various oxygen-containing functional groups of C—O (45.41 %), O—C=O (50.55 %) and C=O (4.04 %), respectively (Barczak et al., 2015). As shown in Fig. 4(d), the spectrum of S 2p can be deconvoluted into three peaks. The peak at 164 eV just splits into two characteristic peaks, namely, 163.98 eV (2p_{3/2}, 50.59 %) and 165.09 eV (2p_{1/2}, 21.86 %). Another fitting peak with higher binding energy (168.58 eV) can be attributed to sulfur oxide (—C—SO_x—C, x = 2,3,4, 27.55 %), which indicates that sulfur atoms are successfully bound to the carbon framework (Chen et al., 2018). Moreover, these electron-withdrawing groups can adjust the charge distribution of adjacent carbon atoms and improve the adsorption capacity of carbon materials for Hg²⁺.

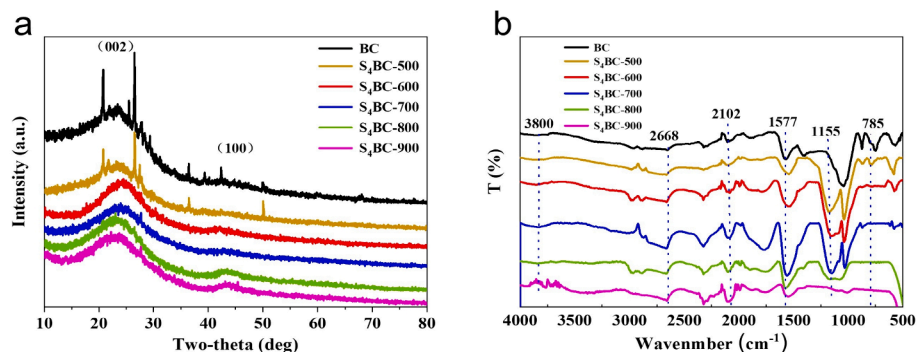


Fig. 3. (a) XRD and (b) FT-IR spectra patterns of BC and S₄BC

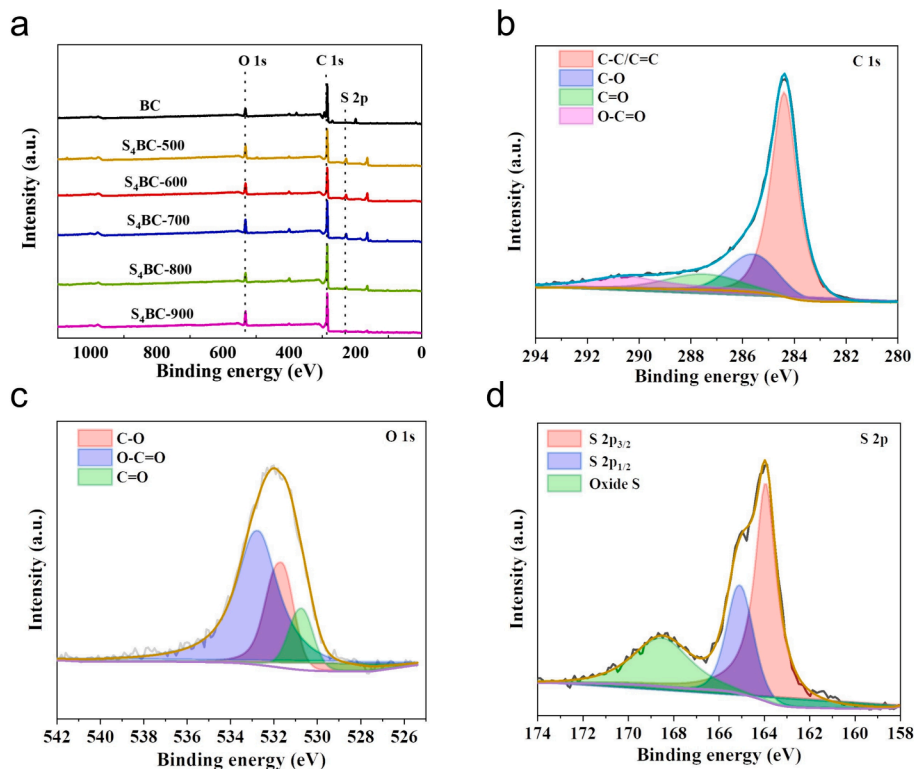


Fig. 4. (a) XPS survey spectra, (b) High-resolution spectra of C 1 s, (c) O 1 s, (d) S 2p of $S_4BC-800$.

3.2. Mercury adsorption performance

3.2.1. Effect of synthesis conditions of materials on Hg^{2+} adsorption

SBC adsorbents synthesized with different amount of $Na_2S_2O_3$ was applied for Hg^{2+} adsorption. The concentration of Hg^{2+} was set at 100 mg/L and the pH value varied from 3 to 7. As shown in Fig. 5(a), as the ratio of BC to $Na_2S_2O_3$ gradually increased from 1:0.5 to 1:4, the adsorption capacity of the prepared materials for Hg^{2+} also gradually increased in the range of pH 3–7. The reason may be that the doped sulfur atoms own the characteristics of large atomic radius, low electronegativity, lone pair electrons for coordination bonds, which can introduce more active sites on the surface of BC. Moreover, due to the high stability constant between S atom and soft acid metal, it greatly contributes to the adsorption of Hg^{2+} by SBC (Lee et al., 2017). Therefore, when the ratio of $Na_2S_2O_3$ is low, less S atoms are doped into carbon frame, resulting in lower adsorption capacity. However, when the ratio further increases from 1:4 to 1:5, the adsorption capacity declines unexpectedly. The reason is that too much $Na_2S_2O_3$ will corrode most

carbon element to produce carbon disulfide and carbon oxide, which leads to the reduction of sulfur content and product yield, thus reducing the adsorption property for Hg^{2+} . Therefore, 1: 4 was chosen as the optimal ratio for the subsequent material preparation.

Activation temperature is another key factor to affect material property, so S_4BC adsorbent prepared under different pyrolysis temperature for Hg^{2+} intake is investigated. As shown in Fig. 5(b), the adsorption properties of all materials are reduced at low pH, which should be attributed to the competitive adsorption of hydrogen ions (Li et al., 2017). With the increase of synthesis temperature from 500 °C to 800 °C, the adsorption capacities of S_4BC exhibit obvious rising trend, and the $S_4BC-800$ owns superior adsorption efficiency to other materials, but it reduces sharply when pyrolysis temperature further increases to 900 °C. The Hg^{2+} adsorption performance on these materials can be well cleared up by above mentioned S content and BET specific surface area (Table 1). The S content of materials under temperature of 500–800 °C exhibit no apparent difference besides of a little fluctuation, but their specific surface area boosts rapidly, so the exposed active sites

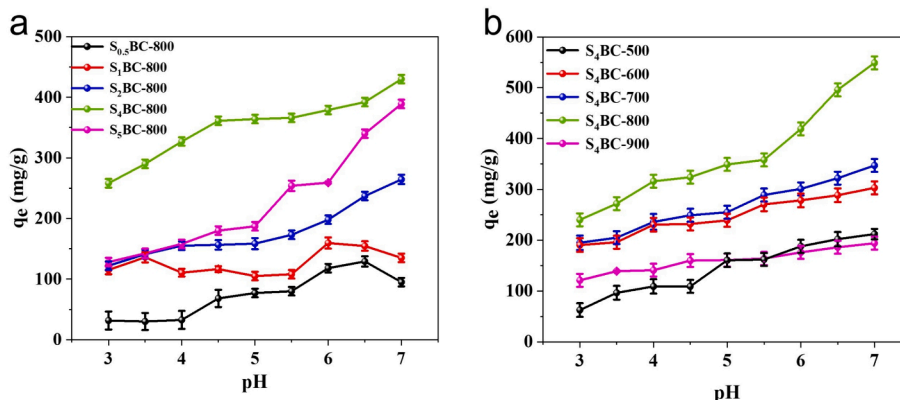


Fig. 5. Hg^{2+} adsorption on (a) $S_xBC-800$ and (b) S_4BC-Y under different solution pH

corresponding to S functional groups will enhance, thus resulting in the increase of adsorption capacity. Although the S₄BC-900 material attained the highest specific surface area of 1303.1 m²/g, the S content decreases sharply from around 20 % to 11.05 %, which may result from decomposition of functional groups containing S element under excessive high temperature. Thus, the reduction of active sites leads to the decrease of adsorption capacity. Based on the above analysis, S₄BC-800 adsorbent is selected for the subsequent experiments. Previous studies have proved that when the pH value exceeds 7, mercury (II) will precipitate in the solution (Inbaraj and Sulochana, 2006), which cannot be clear what causes the disappearance of mercury (II), so we chose 6.5 as the best pH value in the follow-up experiments.

3.2.2. Adsorption isotherms

Adsorption isotherm describes the adsorption behavior of adsorbents for target pollutants at different temperatures and initial concentrations, and adsorption capacity is one of the most important indexes to evaluate adsorbents (dos Reis et al., 2023). In order to study the adsorption isotherm, the initial concentration of Hg²⁺ varied from 20 to 300 mg/L, the temperature was set at 293 K, 303 K and 313 K and the pH value was 6.5. As is shown in Fig. 6(a), the adsorption capacity enhances with the increase of Hg²⁺ concentration, and finally attains equilibrium. The increase of initial metal ions concentration will accelerate the chelation balance between adsorbents and target ions to form coordination compound, thus improving the adsorption capacity (Song et al., 2017). With temperature rising from 293 K to 313 K, the adsorption capacity of S₄BC-800 for Hg²⁺ increase obviously, indicating the endothermic character of the adsorption.

Langmuir and Freundlich adsorption isotherm models were used to fit the equilibrium adsorption data. Langmuir model is usually used for monolayer adsorption, in which a large number of adsorption sites have the same affinity with the adsorbate, while Freundlich model is mainly used to describe heterogeneous adsorption process (Wu et al., 2022). Fig. 6(b) showed the Langmuir linear fitting of Hg²⁺ adsorbed on S₄BC-800 adsorbent, showing a good linear relationship. Table 2 summarizes the relevant parameters and constant values calculated by the above isothermal adsorption equation. It can be seen that R² of Langmuir model is closer to 1 than that of Freundlich model, indicating that Langmuir model is more suitable for fitting adsorption data. It shows that the adsorption of mercury by S₄BC-800 is monolayer adsorption. The maximum adsorption capacity of Hg²⁺ calculated by Langmuir model is 389, 448, and 724 mg/g at 293, 303, and 313 K, respectively, which is higher than that of various adsorbents in Table S3. The results demonstrate that the S₄BC-800 adsorbent possesses great application potential for the elimination of aqueous Hg²⁺ pollutants.

3.2.3. Desorption and regeneration

The regenerative performance is an important factor during practical application of adsorbent (Jiang et al., 2020), and it is very important to achieve efficient reuse after Hg²⁺ adsorption on S₄BC-800. Therefore,

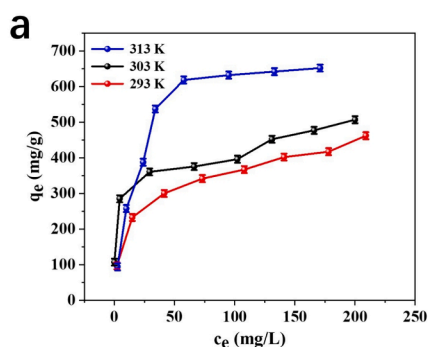


Table 2
Adsorption isotherms parameters of the Langmuir and Freundlich model for the adsorption of Hg²⁺ on S₄BC-800.

Temperature (K)	Langmuir model			Freundlich model		
	θ (mg/g)	b (g/mL)	R^2	K_F (mL ^{1/n} /μg ^{1-1/n})	n	R^2
293	389	0.048	0.992	6.64	3.00	0.968
303	448	0.595	0.998	8.20	2.84	0.850
313	724	0.052	0.998	6.52	2.12	0.882

recycling adsorption experiments were carried out to observe the reusability of S₄BC-800. In order to reuse the adsorbent, it is necessary to effectively desorb the adsorbed Hg²⁺ without destroying the adsorbent. Thus, after each adsorption test, the adsorbent was eluted with 5 mL of 0.2 mol/L HCl containing 3 % thiourea (w/t%), then washed with ultra-pure water and dried in vacuum at 50 °C for reuse. As shown in Fig. 7, the adsorption capacity of the S₄BC-800 was 280 mg/g at the first use, and then decreased to 270 and 260 mg/g at the second and third reuse, respectively, and finally remained stable at the following reuse. When the adsorbent is reused for the first and second time, the adsorption capacity of Hg²⁺ exhibits a slight decrease, which may result from the loss of a small number of sulfur-containing groups that are not firmly fixed on the adsorbent. The remaining sulfur-containing groups are firmly combined with the material and are not easily destroyed by eluent, so the adsorption capacity remains unchanged in the subsequent reuse process. After recycling for 6 times, the adsorption capacity still maintained over 250 mg/g, which showed that the S₄BC-800 adsorbent

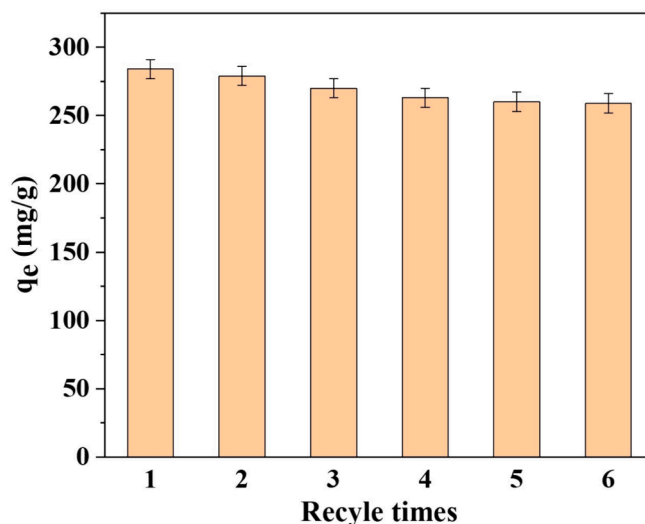


Fig. 7. Effect of S₄BC-800 reuse on Hg²⁺ adsorption capacity.

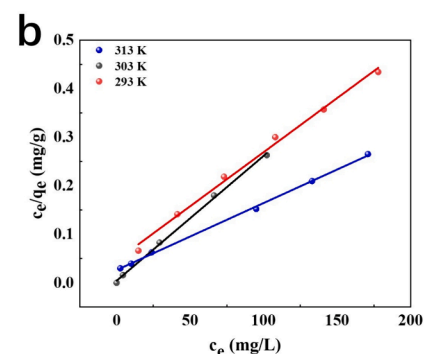


Fig. 6. (a) Adsorption isotherm of Hg²⁺ by S₄BC-800 (b) Fitting curve of adsorption isotherm of pollutants by S₄BC-800.

owned good reusability and great practical application potential.

3.3. Adsorption mechanism and environmental significance

In order to understand the adsorption mechanism, the XPS analysis of S₄BC-800 adsorbed Hg²⁺ was carried out. It can be seen from Fig. 8(a) that two Hg 4f peaks after adsorption are clearly displayed in the survey spectrum, indicating that a large amount of Hg²⁺ are adsorbed on S₄BC-800. Specifically, as shown in Fig. 8(b), two peaks at 104.95 eV and 101.07 eV belong to Hg 4f_{7/2} and Hg 4f_{5/2}, which proves that Hg exists in its metallic form. Therefore, the result shows that Hg²⁺ is reduced to Hg(0) at a certain moment in the adsorption process (Arshadi et al., 2018). In Fig. 8(c), however, the binding energy peaks of O 1s atoms move from 530.68, 531.78, and 532.68 eV to 531.74, 532.58, and 532.83 eV, which shows that oxygen-containing groups play a role in Hg²⁺ removal by electrostatic interaction between oppositely charged ions. That is, positively charged functional groups can interact with Hg²⁺ through cation exchange reaction (Bao et al., 2017). In Fig. 8(d), after adsorption of Hg²⁺, the binding energy of S 2p shifts from 164.00 eV to 164.56 eV, and the alteration is due to the sharing of lone pair electrons S atoms with Hg²⁺ (Zhang et al., 2013). According to the HSAB, soft base can combine with soft acid to form a stable complex. Hg²⁺ has relatively large ionic size, low electronegativity and high polarizability, which are all characteristics of soft acids (Hakami et al., 2012), while as a soft base, sulfur atoms with lone electron pairs belong to soft Lewis base sites (Wang et al., 2019b). Therefore, the basic sulfur groups have strong coordination with acidic Hg²⁺, and it is easy to form strong Hg-S bonds through covalent bonds (Delacote et al., 2009; Ram and Chauhan, 2018; Wajima and Sugawara, 2011), which leads to the decrease of the contents of S 2p_{3/2} and S 2p_{1/2} from 50.59 % and 21.86 % to 46.92 % and 17.75 % respectively. However, the —C—SO_x—C in S₄BC-800 increased from 27.55 % to 35.33 %, which indicated that the sulfur oxides produced during adsorption adhered to the surface of

S₄BC-800. Based on the above results, we can conclude that the adsorption of Hg²⁺ on S₄BC-800 material is a chemical adsorption process, which is driven by coordination, ion exchange, and electrostatic interaction between the oxygen and sulfur-containing groups of S₄BC-800 material and Hg²⁺.

Although the S₄BC-800 material exhibits excellent adsorption performance, its feasibility for low level Hg²⁺, which usually presents in actual polluted water, and dynamic operation should be further examined. Thus, a microfiltration membrane device base on S₄BC-800 (Fig. 9a) has been designed for removal of low concentration of Hg²⁺ (10 µg/L), and the results are shown in Fig. 9(b). When Hg²⁺ solution passes through PVDF membrane without S₄BC-800, the removal rate of Hg²⁺ is almost negligible, indicating that PVDF membrane hardly adsorbs Hg²⁺. When Hg²⁺ solution passes through the PVDF membrane supported by S₄BC-800, most of Hg²⁺ is adsorbed on S₄BC-800, showing excellent adsorption performance for low concentration Hg²⁺. It shows that even after 1 L water sample passes through the membrane, the residual Hg²⁺ concentration of the filter membrane loaded with 0.4 g S₄BC-800 is still zero. With the increase of water sample loading, the residual Hg²⁺ in the filter membrane loaded with 0.05 g and 0.1 g adsorbents increase slightly by 3.3 and 1.8 µg/L, respectively, which were far below the maximum allowable concentration of total mercury (50 µg/L) in the comprehensive wastewater discharge standard of China (Liu et al., 2021). Although the water sample stays in the active layer of the membrane for a short time, it can still obtain high removal efficiency of Hg²⁺, which is attributed to the excellent adsorption capacity and rapid adsorption rate of S₄BC-800. The feasibility of the designed water treatment device based on S₄BC-800 adsorbent provides a beneficial exploration for the purification of Hg²⁺ polluted water (Fig. 10).

4. Conclusion

SBC material was successfully synthesized with cherry kernel powder

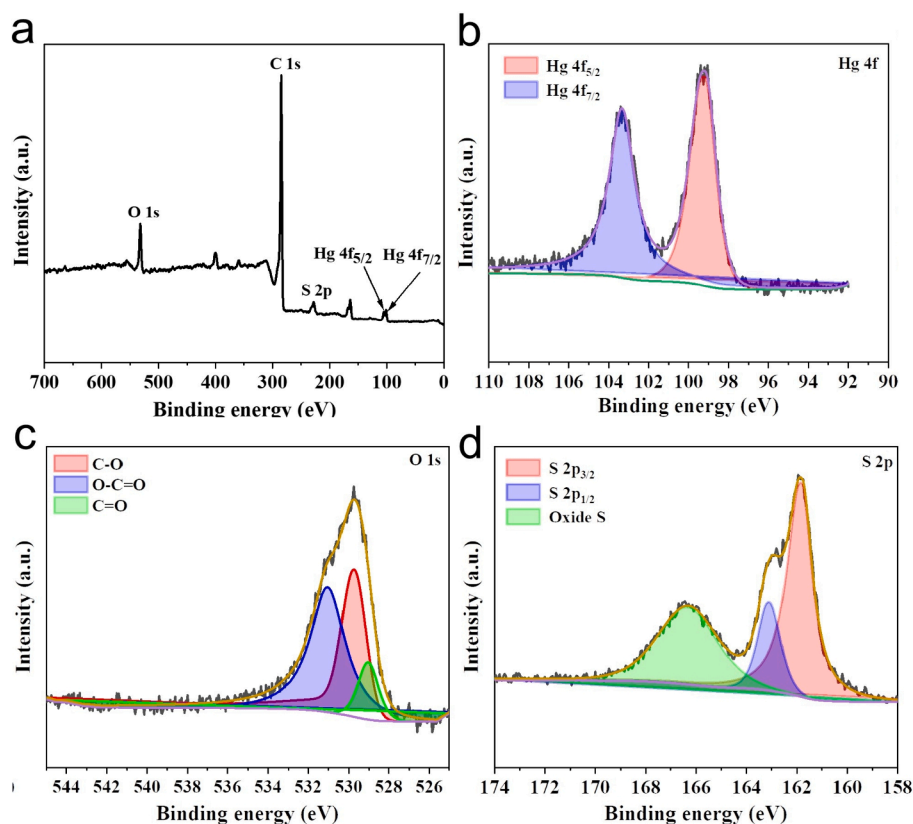


Fig. 8. (a) XPS survey spectra of used S₄BC-800. High-resolution (b) Hg 4f(c) O 1s and (d) S 2p spectra of used S₄BC-800.

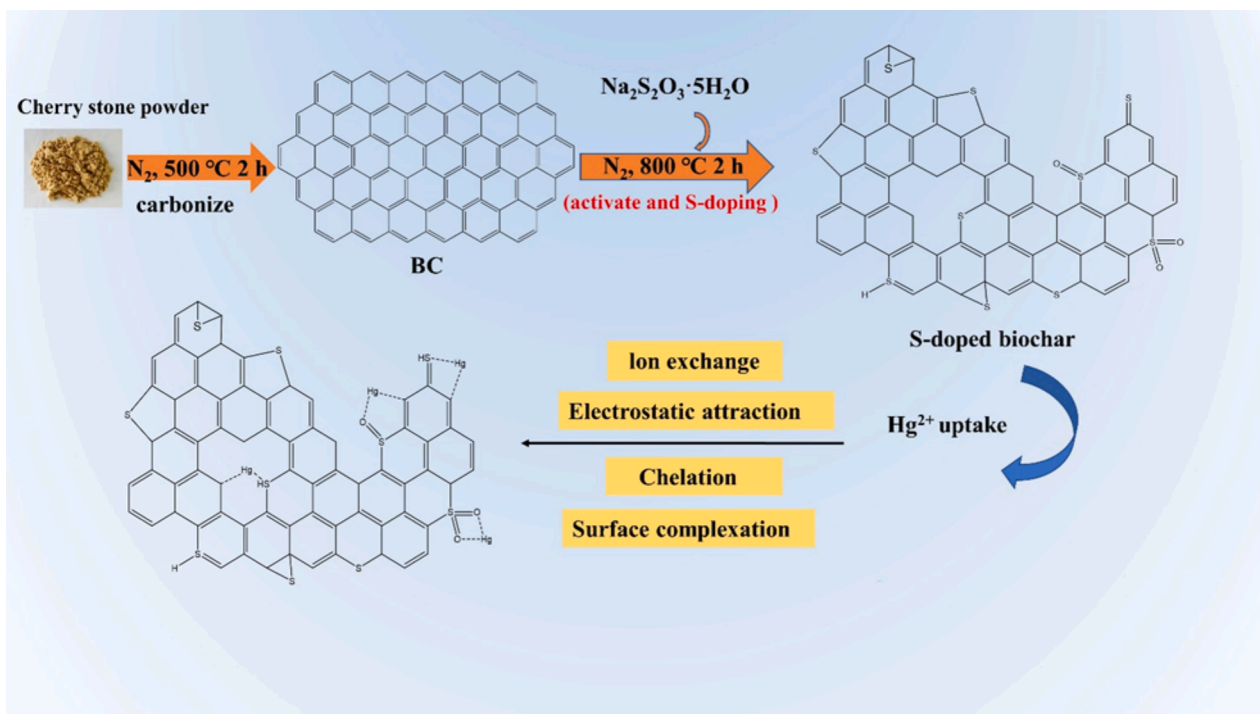


Fig. 9. Adsorption mechanism schematic diagram of $S_4BC-800$ for Hg^{2+} .

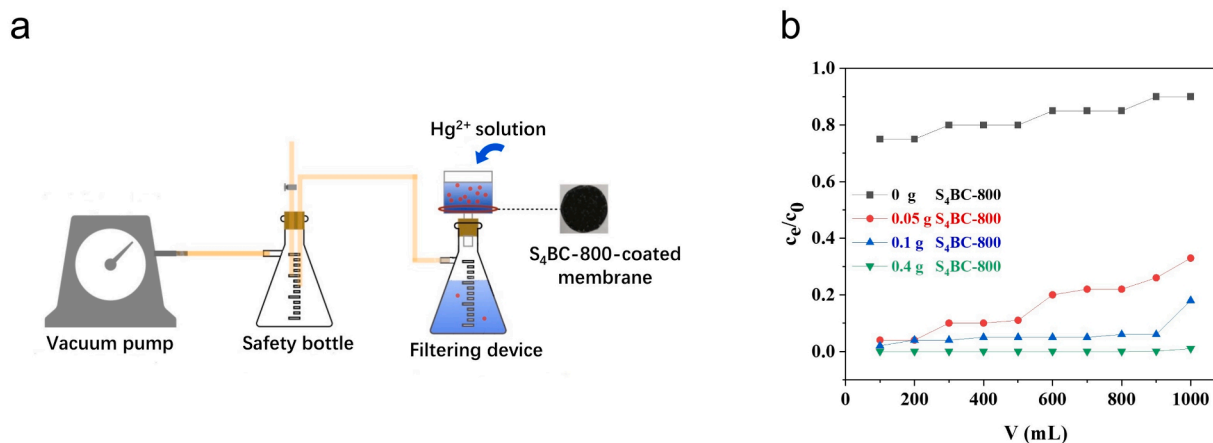


Fig. 10. (a) Membrane filtration system, (b) Hg^{2+} removal performance of $S_4BC-800$ /PVDF membrane

as carbon source and $Na_2S_2O_3$ as activating reagent and sulfur source. The material prepared at $800\text{ }^\circ\text{C}$ with appropriate mass ratio of biochar to $Na_2S_2O_3 \cdot 5H_2O$ (1:4) exhibited the optimal adsorption performance for Hg^{2+} . Adsorption kinetics demonstrated the rapid adsorption of Hg^{2+} by $S_4BC-800$, and the pseudo-second-order kinetic model could fit the adsorption data well. The isotherm study showed that the adsorption of Hg^{2+} was in accord with Langmuir model and owned high adsorption capacity. The microfiltration membrane device based on $S_4BC-800$ has good removal performance for low concentration of Hg^{2+} under dynamic adsorption process. The study of adsorption mechanism shows that the combination of Hg^{2+} and $S_4BC-800$ is mainly driven by electrostatic interaction and coordination with sulfur-containing groups. However, in the follow-up study, it is necessary to further explore the surface active center and adsorption mechanism of Hg^{2+} by combining in-situ characterization and theoretical calculation, so as to deepen the understanding of sulfur doping to improve the performance of biochar.

CRediT authorship contribution statement

Zengrun Xie: Writing – review & editing, Writing – original draft, Supervision, Resources, Project administration. **Yuanyuan Zhang:** Methodology. **Shengxiao Zhang:** Funding acquisition. **Hou Chen:** Resources. **Chenyu Du:** Methodology. **Caijuan Zhong:** Supervision.

Declaration of competing interest

The authors declare that they have no known competing financial interests or personal relationships that could have appeared to influence the work reported in this paper.

Acknowledgements

This study was co-supported by the Science and Technology Innovation Development Program of Yantai (2022XDRH009, 2023ZLYJ118),

the Science Fund of Shandong Laboratory of Advanced Materials and Green Manufacturing at Yantai (AMGM2024F13), and the Innovation Project for graduate students of Ludong University (IPGS2024-055).

Appendix A. Supplementary material

Supplementary material to this article can be found online at <https://doi.org/10.1016/j.arabjc.2024.105955>.

References

- Abbas, K., Znad, H., Awual, M.R., 2018. A ligand anchored conjugate adsorbent for effective mercury(II) detection and removal from aqueous media. *Chem. Eng. J.* 334, 432–443.
- Arshadi, M., Eskandarloo, H., Abdolmaleki, M.K., Abbaspourrad, A., 2018. A biocompatible nanodendrimer for efficient adsorption and reduction of Hg(II). *ACS Sustainable Chem. Eng.* 6, 13332–13348.
- Bao, S., Li, K., Ning, P., Peng, J., Jin, X., Tang, L., 2017. Highly effective removal of mercury and lead ions from wastewater by mercaptoamine-functionalised silica-coated magnetic nano-adsorbents: Behaviours and mechanisms. *Appl. Surf. Sci.* 393, 457–466.
- Barczak, M., Michalak-Zwierz, K., Gdula, K., Tyszczyk-Rotko, K., Dobrowolski, R., Nbrowski, A., 2015. Ordered mesoporous carbons as effective sorbents for removal of heavy metal ions. *Micropor. Mesopor. Mater.* 211, 162–173.
- Castro-Munoz, R., Gonzalez-Melgoza, L.L., Garcia-Depraect, O., 2021. Ongoing progress on novel nanocomposite membranes for the separation of heavy metals from contaminated water. *Chemosphere* 270, 129421.
- Chen, H., Yu, F., Wang, G., Chen, L., Dai, B., Peng, S.L., 2018. Nitrogen and sulfur self-doped activated carbon directly derived from elm flower for high-performance supercapacitors. *ACS Omega* 3, 4724–4732.
- Clarkson, T.W., Magos, L., 2006. The toxicology of mercury and its chemical compounds. *Crit. Rev. Toxicol.* 36, 609–662.
- Correa, C.R., Stollovsky, M., Hehr, T., Rauscher, Y., Rolli, B., Kruse, A., 2017. Influence of the carbonization process on activated carbon properties from lignin and lignin-rich biomasses. *ACS Sustainable Chem. Eng.* 5, 8222–8233.
- Delacote, C., Gaslain, F.O., Lebeau, B., Walcarius, A., 2009. Factors affecting the reactivity of thiol-functionalized mesoporous silica adsorbents toward mercury(II). *Talanta* 79, 877–886.
- dos Reis, G.S., Dotto, G.L., Vieillard, J., Oliveira, M.L.S., Lütke, S.F., Grimm, A., Silva, L.F.O., Lima, É.C., Naushad, M., Lassi, U., 2023. Nickel-aluminium layered double hydroxide as an efficient adsorbent to selectively recover praseodymium and samarium from phosphogypsum leachate. *J. Alloys Compd.* 960.
- dos Reis, S.G., Grimm, A., Fungaro, D.A., Hu, T., de Brum, I.A.S., Lima, E.C., Naushad, M., Dotto, G.L., Lassi, U., 2024. Synthesis of sustainable mesoporous sulfur-doped bio-based carbon with superior performance sodium diclofenac removal: Kinetic, equilibrium, thermodynamic and mechanism. *Environ. Res.* 251.
- dos Reis, G.S., Larsson, S.H., Mathieu, M., Thyrel, M., Pham, T.N., 2021. Application of design of experiments (DoE) for optimised production of micro- and mesoporous Norway spruce bark activated carbons. *Biomass Convers. Biorefinery* 13, 10113–10131.
- Fu, K., Liu, X., Lv, C., Luo, J., Sun, M., Luo, S., Crittenden, J.C., 2022. Superselective Hg (II) removal from water using a thiol-laced MOF-based sponge monolith: Performance and mechanism. *Environ. Sci. Technol.* 56, 2677–2688.
- Giri, D.D., Jha, J.M., Tiwari, A.K., Srivastava, N., Hashem, A., Alqarawi, A.A., Abd Allah, E.F., Pal, D.B., 2021. Java plum and amalash seed biomass based bio-adsorbents for synthetic wastewater treatment. *Environ. Pollut.* 280, 116890.
- Godlewska, P., Siatecka, A., Kończak, M., Oleszczuk, P., 2019. Adsorption capacity of phenanthrene and pyrene on engineered carbon-based adsorbents produced from sewage sludge or sewage sludge-biomass mixture in various gaseous conditions. *Bioresour. Technol.* 280, 421–429.
- Guo, Y.P., Zeng, Z.Q., Li, Y.L., Huang, Z.G., Yang, J.Y., 2017. Catalytic oxidation of 4-chlorophenol on in-situ sulfur-doped activated carbon with sulfate radicals. *Sep. Purif. Technol.* 179, 257–264.
- Guo, Y., Zeng, Z., Zhu, Y., Huang, Z., Cui, Y., Yang, J., 2018. Catalytic oxidation of aqueous organic contaminants by persulfate activated with sulfur-doped hierarchically porous carbon derived from thiophene. *Appl. Catal. B-Environ.* 220, 635–644.
- Hakami, O., Zhang, Y., Banks, C.J., 2012. Thiol-functionalised mesoporous silica-coated magnetite nanoparticles for high efficiency removal and recovery of Hg from water. *Water Res.* 46, 3913–3922.
- He, J.W., Long, Y., Wang, Y.Y., Wei, C.L., Zhan, J.J., 2016. Aerosol-assisted self-assembly of reticulated N-doped carbonaceous submicron spheres for effective removal of hexavalent chromium. *ACS Appl. Mater. Interfaces* 8, 16699–16707.
- Hu, S.C., Cheng, J., Wang, W.P., Sun, G.T., Hu, L.L., Zhu, M.Q., Huang, X.H., 2021. Structural changes and electrochemical properties of lacquer wood activated carbon prepared by phosphoric acid-chemical activation for supercapacitor applications. *Renew. Energ.* 177, 82–94.
- Hussain, I., Qi, J.W., Sun, X.Y., Wang, L.J., Li, J.S., 2020. Melamine derived nitrogen-doped carbon sheet for the efficient removal of chromium (VI). *J. Mol. Liq.* 318, 114052.
- Inbaraj, B., Sulochana, N., 2006. Mercury adsorption on a carbon sorbent derived from fruit shell of Terminalia catappa. *J. Hazard. Mater.* 133, 283–290.
- Jiang, C.L., Wang, X.H., Hou, B.X., Hao, C., Li, X., Wu, J.B., 2020. Construction of a lignosulfonate-lysine hydrogel for the adsorption of heavy metal ions. *J. Agric. Food Chem.* 68, 3050–3060.
- Kou, D.H., Ma, W., Zhang, S.F., 2021. Functionalized mesoporous photonic crystal film for ultrasensitive visual detection and effective removal of mercury (II) ions in water. *Adv. Funct. Mater.* 31, 2007032.
- Lee, J.S.M., Parker, D.J., Cooper, A.L., Hasell, T., 2017. High surface area sulfur-doped microporous carbons from inverse vulcanised polymers. *J. Mater. Chem. A* 5, 18603–18609.
- Li, J.X., Jiang, B.Q., Liu, Y., Qiu, C.Q., Hu, J.J., Qian, G.R., Guo, W.S., Ngo, H.H., 2017. Preparation and adsorption properties of magnetic chitosan composite adsorbent for Cu²⁺ removal. *J. Clean. Prod.* 158, 51–58.
- Li, D.H., Li, L.Q., Chen, R.F., Wang, C.H., Li, H.L., Li, H.Y., 2018a. A MIL-101 composite doped with porous carbon from tobacco stem for enhanced acetone uptake at normal temperature. *Ind. Eng. Chem. Res.* 57, 6226–6235.
- Li, L.Q., Ma, X.C., Chen, R.F., Wang, C.H., Lu, M.M., 2018b. Nitrogen-containing functional groups-facilitated acetone adsorption by ZIF-8-derived porous carbon. *Materials* 11, 159.
- Li, Y.J., Wang, G.L., Wei, T., Fan, Z.J., Yan, P., 2016. Nitrogen and sulfur co-doped porous carbon nanosheets derived from willow catkin for supercapacitors. *Nano Energy* 19, 165–175.
- Liang, S.-X., Duan, F.-F., Lü, Q.-F., Yang, H., 2019. Hierarchical biocarbons with controlled micropores and mesopores derived from kapok fruit peels for high-performance supercapacitor electrodes. *ACS Omega* 4, 5991–5999.
- Liu, S., Liang, Y., Zhou, W., Hu, W., Dong, H., Zheng, M., Hu, H., Lei, B., Xiao, Y., Liu, Y., 2018b. Large-scale synthesis of porous carbon via one-step CuCl₂ activation of rape pollen for high-performance supercapacitors. *J. Mater. Chem. A* 6, 12046–12055.
- Liu, C., Peng, J., Zhang, L., Wang, S., Ju, S., Liu, C., 2018a. Mercury adsorption from aqueous solution by regenerated activated carbon produced from depleted mercury-containing catalyst by microwave-assisted decontamination. *J. Cleaner Prod.* 196, 109–121.
- Liu, S.J., Wang, X.D., Guo, G.L., Yan, Z.G., 2021. Status and environmental management of soil mercury pollution in China: A review. *J. Environ. Manage.* 277, 111442.
- Ma, X.Y., Cao, M.H., Hu, C.W., 2013. Bifunctional HNO₃ catalytic synthesis of N-doped porous carbons for CO₂ capture. *J. Mater. Chem. A* 1, 913–918.
- Ma, G.X., Ning, G.Q., Wei, Q., 2022. S-doped carbon materials: Synthesis, properties and applications. *Carbon* 195, 328–340.
- Park, J.E., Jang, Y.J., Kim, Y.J., Song, M.S., Yoon, S., Kim, D.H., Kim, S.J., 2014. Sulfur-doped graphene as a potential alternative metal-free electrocatalyst and Pt-catalyst supporting material for oxygen reduction reaction. *Phys. Chem. Chem. Phys.* 16, 103–109.
- Pearson, R.G., 1963. Hard and Soft Acids and Bases. *J. Am. Chem. Soc.* 85, 3533–3539.
- Qu, J., Akindolie, M.S., Feng, Y., Jiang, Z., Zhang, G., Jiang, Q., Deng, F., Cao, B., Zhang, Y., 2020. One-pot hydrothermal synthesis of NaLa(CO₃)₂ decorated magnetic biochar for efficient phosphate removal from water: Kinetics, isotherms, thermodynamics, mechanisms and reusability exploration. *Chem. Eng. J.* 394, 124915.
- Qu, J., Wang, Y., Tian, X., Jiang, Z., Deng, F., Tao, Y., Jiang, Q., Wang, L., Zhang, Y., 2021. KOH-activated porous biochar with high specific surface area for adsorptive removal of chromium (VI) and naphthalene from water: Affecting factors, mechanisms and reusability exploration. *J. Hazard. Mater.* 401.
- Ram, B., Chauhan, G.S., 2018. New spherical nanocellulose and thiol-based adsorbent for rapid and selective removal of mercuric ions. *Chem. Eng. J.* 331, 587–596.
- Saleem, H., Pal, P., Hajja, M.A., Banat, F., 2019. Regeneration and reuse of bio-surfactant to produce colloidal gas aphrons for heavy metal ions removal using single and multistage cascade flotation. *J. Clean. Prod.* 217, 493–502.
- Seredych, M., Bandoz, T.J., 2011. Investigation of the enhancing effects of sulfur and/or oxygen functional groups of nanoporous carbons on adsorption of dibenzothiophenes. *Carbon* 49, 1216–1224.
- Song, X.T., Niu, Y.Z., Qiu, Z.M., Zhang, Z.X., Zhou, Y.Z., Zhao, J.J., Chen, H., 2017. Adsorption of Hg(II) and Ag(I) from fuel ethanol by silica gel supported sulfur-containing PAMAM dendrimers: Kinetics, equilibrium and thermodynamics. *Fuel* 206, 80–88.
- Srinivasan, R., Elaiyappillai, E., Pandian, H.P., Vengudusamy, R., Johnson, P.M., Chen, S.M., Karvembu, R., 2019. Sustainable porous activated carbon from Polyalthia longifolia seeds as electrode material for supercapacitor application. *J. Electroanal. Chem.* 849, 113382.
- Uygun, A., Yavuz, A.G., Sen, S., Omastová, M., 2009. Polythiophene/SiO₂ nanocomposites prepared in the presence of surfactants and their application to glucose biosensing. *Synthetic. Met.* 159, 2022–2028.
- Vikrant, K., Kim, K.H., 2019. Nanomaterials for the adsorptive treatment of Hg(II) ions from water. *Chem. Eng. J.* 358, 264–282.
- Wajima, T., Sugawara, K., 2011. Adsorption behaviors of mercury from aqueous solution using sulfur-impregnated adsorbent developed from coal. *Fuel Process. Technol.* 92, 1322–1327.
- Wang, S.R., Dai, G.X., Yang, H.P., Luo, Z.Y., 2017. Lignocellulosic biomass pyrolysis mechanism: A state-of-the-art review. *Prog. Energ. Combust.* 62, 33–86.
- Wang, X.B., Qin, Y.L., Zhu, L.H., Tang, H.Q., 2015. Nitrogen-doped reduced graphene oxide as a bifunctional material for removing bisphenols: Synergistic effect between adsorption and catalysis. *Environ. Sci. Technol.* 49, 6855–6864.
- Wang, L.Z., Wang, J.J., Wang, Y., Zhou, F., Huang, J.H., 2022. Thioether-functionalized porphyrin-based polymers for Hg²⁺ efficient removal in aqueous solution. *J. Hazard. Mater.* 429, 128303.
- Wang, X., Yang, C., Xiong, X., Chen, G., Huang, M., Wang, J.-H., Liu, Y., Liu, M., Huang, K., 2019b. A robust sulfur host with dual lithium polysulfide immobilization

- mechanism for long cycle life and high capacity Li-S batteries. *Energy Storage Mater.* 16, 344–353.
- Wang, Q., Yu, J., Chen, X., Du, D., Wu, R., Qu, G., Guo, X., Jia, H., Wang, T., 2019a. Non-thermal plasma oxidation of Cu(II)-EDTA and simultaneous Cu(II) elimination by chemical precipitation. *J. Environ. Manage.* 248, 109237.
- Wepasnick, K.A., Smith, B.A., Schrote, K.E., Wilson, H.K., Diegelmann, S.R., Fairbrother, D.H., 2011. Surface and structural characterization of multi-walled carbon nanotubes following different oxidative treatments. *Carbon* 49, 24–36.
- Wu, T., Liu, C., Kong, B., Sun, J., Gong, Y.J., Liu, K., Xie, J., Pei, A., Cui, Y., 2019. Amidoxime-functionalized macroporous carbon self-refreshed electrode materials for rapid and high-capacity removal of heavy metal from water. *ACS Central Sci.* 5, 719–726.
- Wu, K., Wang, B., Tang, B., Luan, L., Xu, W., Zhang, B., Niu, Y., 2022. Adsorption of aqueous Cu(II) and Ag(I) by silica anchored Schiff base decorated polyamidoamine dendrimers: Behavior and mechanism. *Chin. Chem. Lett.* 33, 2721–2725.
- Yang, Q., Wang, H.L., Li, F.B., Dang, Z., Zhang, L.J., 2021. Rapid and efficient removal of Cr(VI) by a core-shell magnetic mesoporous polydopamine nanocomposite: Roles of the mesoporous structure and redox-active functional groups. *J. Mater. Chem. A* 9, 13306–13319.
- Yang, Z., Yao, Z., Li, G.F., Fang, G.Y., Nie, H.G., Liu, Z., Zhou, X.M., Chen, X., Huang, S.M., 2012. Sulfur-doped graphene as an efficient metal-free cathode catalyst for oxygen reduction. *ACS Nano* 6, 205–211.
- Yang, L.X., Zhang, Y.Y., Wang, F.F., Luo, Z.D.E., Guo, S.J., Strahle, U., 2020. Toxicity of mercury: Molecular evidence. *Chemosphere* 245, 35.
- Yilmaz, F.M., Gorguc, A., Karaaslan, M., Vardin, H., Bilek, S.E., Uygun, O., Bircan, C., 2019. Sour cherry by-products: Compositions, functional properties and recovery potentials – A review. *Crit. Rev. Food Sci.* 59, 3549–3563.
- Zeng, H.P., Yin, C., Qiao, T.D., Yu, Y.P., Zhang, J., Li, D., 2018. As(V) removal from water using a novel magnetic particle adsorbent prepared with iron-containing water treatment residuals. *ACS Sustainable Chem. Eng.* 6, 14734–14742.
- Zhang, S., Zhang, Y., Liu, J., Xu, Q., Xiao, H., Wang, X., Xu, H., Zhou, J., 2013. Thiol modified Fe₃O₄@SiO₂ as a robust, high effective, and recycling magnetic sorbent for mercury removal. *Chem. Eng. J.* 226, 30–38.
- Zheng, J.J., Wang, Z.W., Ma, J.X., Xu, S.P., Wu, Z.C., 2018. Development of an electrochemical ceramic membrane filtration system for efficient contaminant removal from waters. *Environ. Sci. Technol.* 52, 4117–4126.